Supporting Information

Correlations between Transition Metal Chemistry, Local Structure and Global Structure in $Li_2Ru_{0.5}Mn_{0.5}O_3$ Investigated in a Wide Voltage Window

Yingchun Lyu[†,⊥], Enyuan Hu[‡], Dongdong Xiao[†], Yi Wang[†], Xiqian Yu[*,†], Guiliang Xu[§], Steven N. Ehrlich[¶], Khalil Amine[§], Lin Gu[*,†,∥], Xiao-Qing Yang[‡] and Hong Li[*,†]

[†] Beijing National Laboratory for Condensed Matter Physics, Institute of Physics, Chinese Academy of Sciences, Beijing 100190, China

[‡] Chemistry Division, Brookhaven National Laboratory, Upton, NY 11973, USA

[§] Chemical Sciences and Engineering Division, Argonne National Laboratory, Argonne, IL 60439, USA

[⊥] Materials Genome Institute, Shanghai University, Shanghai 200444, China

[∥] Collaborative Innovation Center of Quantum Matter, Beijing 100190, China

[¶] NSLS-II, Brookhaven National Laboratory, Upton, NY 11973, USA

■ EXPERIMENTAL SECTION

Sample preparation. The $Li_2Ru_{0.5}Mn_{0.5}O_3$ and Li_2RuO_3 samples were prepared by a solid state reaction as described previously.[1] In brief, Li_2CO_3 (Alfa Aesar, 99%), $MnCO_3$ (Alfa Aesar, 99.9%), and RuO_2 (Alfa Aesar, 99.9%) (5 wt. % excess of Li_2CO_3 was used in order to compensate for the loss of Li) were mixed by hand grinding for 1 hour. The resulting mixture was heated at 900 °C for 15 hours and 950 °C for 15 hours with an intermediate grinding for 30 minutes. The heating and cooling rates were maintained at 2 °C min^{-1}.

Powder XRD. X-ray powder diffraction (XRD) patterns were recorded in the range of 15-80° using a Bruker D8 Advance diffractometer equipped with a Cu K_α radiation source (λ_1 = 1.54060 Å, λ_2 = 1.54439 Å) and a LynxEye_XE detector. The powder patterns were refined using TOPAS software based on the Rietveld method.

Electrochemical Measurements. The charge/discharge tests were performed with a Swagelok-type cell. The cells were cycled in the voltage range of 1-4.6 V to evaluate the electrochemical performances of $Li_2Ru_{0.5}Mn_{0.5}O_3$. The working electrode was prepared by spreading the slurry of the active material $Li_2Ru_{0.5}Mn_{0.5}O_3$, conductive agent (acetylene black), and poly(vinylidenedifluoride) (PVDF) in a weight ratio of 80:10:10 onto an aluminum foil current collector. Metallic lithium was used as a counter electrode. A glass microfiber filter (Whatman GF/D) was used as a separator. The electrolyte solution was 1 M $LiPF_6$ in ethylene carbonate (EC) and dimethyl carbonate (DMC) (1:1 by volume). The galvanostatic charge and discharge experiment was performed on a Land automatic battery test system (LAND, China) at room temperature. The galvanostatistic intermittent titration technique (GITT) measurement was employed at a pulse of 68 μA (C/10) for 1 hour with 24 hours interruption between each pulse on an Arbin battery test system (Arbin Instruments, US) at room temperature.

***In situ* XRD measurement.** The working electrode was prepared using polytetrafluoroethylene (PTFE) as a binder. A specially designed Swagelok-type cell with an X-ray-transparent beryllium window was used for the *in situ* measurement. The *in situ* XRD patterns were collected with an interval of 30 minutes for each 2θ scan on charge and discharge at a C/20 rate, between 1 and 4.6

V vs. Li^+/Li.

***In situ* and *ex situ* Synchrotron X-ray absorption spectroscopy.** *In situ* hard X-ray absorption spectroscopy (XAS) experiments were carried out on beamline X18A of the National Synchrotron Light Source (NSLS) at Brookhaven National Laboratory. *Ex situ* measurements were carried out on beamline BL14W1 of the Shanghai Synchrotron Radiation Facility (SSRF). For the experiments at NSLS, the station was operated with a Si (111) double crystal monochromator. A reference spectrum for each element was simultaneously collected using a transition metal foil with the corresponding spectrum collected from the *in situ* cells. Energy calibration was carried out using the first inflection point of the K-edge spectrum of transition metal foil. Analysis of the XAS spectra was carried out by the program code IFEFFIT.[2] The qualitative observations of the as-prepared $Li_2Ru_{0.5}Mn_{0.5}O_3$ were confirmed by quantitative analysis of the extended X-ray absorption fine structure (EXAFS) spectra to obtain structural parameters. This analysis is performed by least-squares fits of phase and amplitude functions, generated by the FEFF 6 code. Li_2MnO_3 (space group: *C2/m*) and Li_2MnO_3 (space group: *C2/m*)/Li_2RuO_3 (space group: $P2_1/m$) were chosen as initial model to fit Mn and Ru FT-EXAFS respectively. The first two peaks of the Ru and Mn FT-EXAFS were fitted. The detailed fitting parameters are presented in Table S1.

Ex Situ PDF characterization. *Ex situ* pair distribution function measurements were carried out at beamline 28-ID-2 (NSLS-II, United States), with a photon wavelength of 0.185794 Å. A large-area amorphous-silicon-based detector was used to collect data to high values of momentum transfer (Qmax = 23.5 $Å^{-1}$). The software FIT2d[3] was used to integrate the raw images. Analyses of the PDF data were carried out by the program code PDFgetX3.[4]

***Ex situ* synchrotron XRD.** The synchrotron radiation *ex situ* XRD was collected at beamline 17-BM-B ((λ = 0.7277 Å) of the Advanced Photon Sources, Argonne National Laboratory (APS, ANL).

HAADF-STEM. Aberration-corrected high-angle annular-dark-field scanning transmission electron microscopy (HAADF-STEM) was performed using a JEOL ARM 200F (JEOL, Tokyo,

Japan) transmission electron microscope at 200 keV. The attainable spatial resolution of the microscope is 80 picometre at an incident angle of 40 mrad. To simulate the STEM images, crystal structure models were created in VESTA.[5] HAADF-STEM images were analyzed by a fast Fourier transform technique, which also reduced the noise of the images.

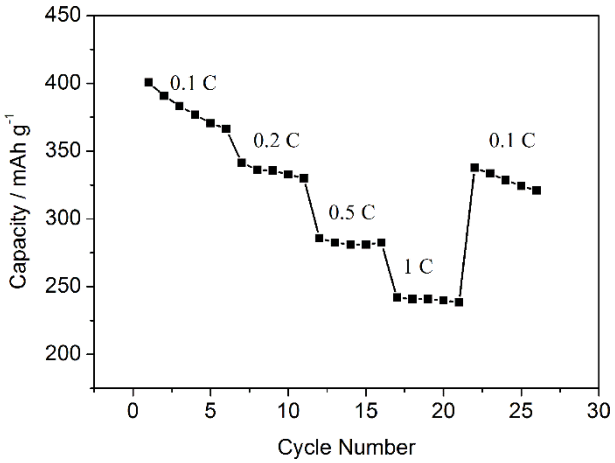

Figure S1. The rate performance of the $Li_2Ru_{0.5}Mn_{0.5}O_3$/Li cell cycled in voltage range of 1.0-4.6 V.

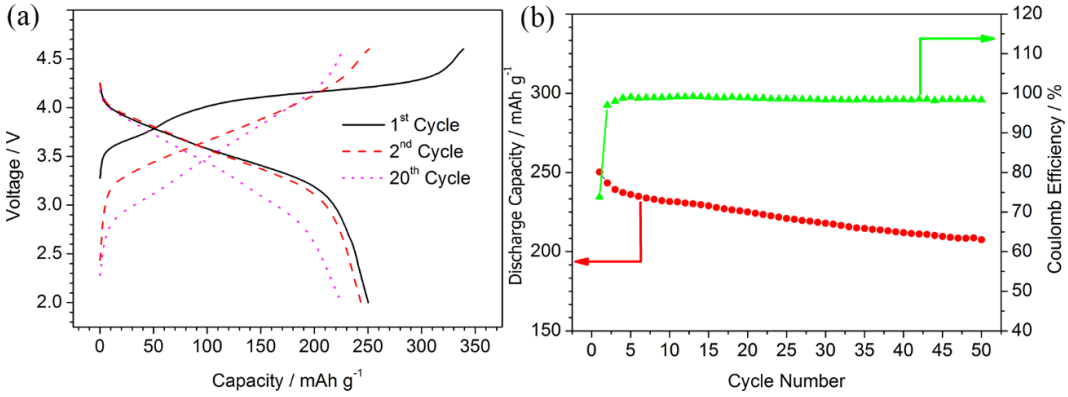

Figure S2. (a) The charge and discharge voltage profiles of the $Li_2Ru_{0.5}Mn_{0.5}O_3$/Li cell at the 1st, 2nd and 20th cycled in the voltage range of 2-4.6 V. (b)The corresponding cycle performance and coulumbic efficiency of the cell for the first 50 cycles.

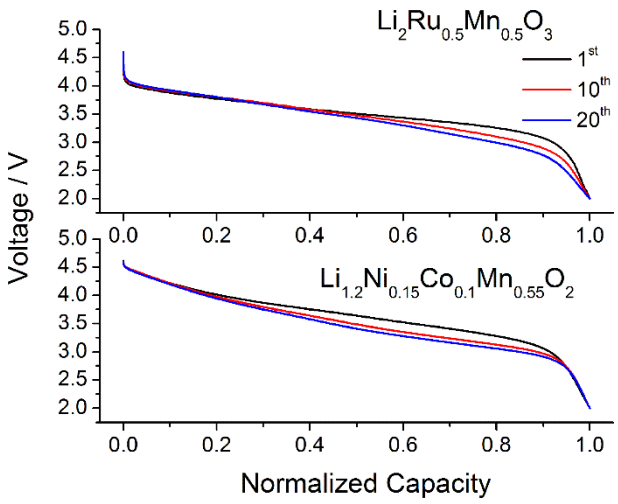

Figure S3. Comparison of the discharge profiles between $Li_2Ru_{0.5}Mn_{0.5}O_3$ and Li rich NMC type $Li_{1.2}Ni_{0.15}Co_{0.1}Mn_{0.55}O_2$[6] with normalized capacity.

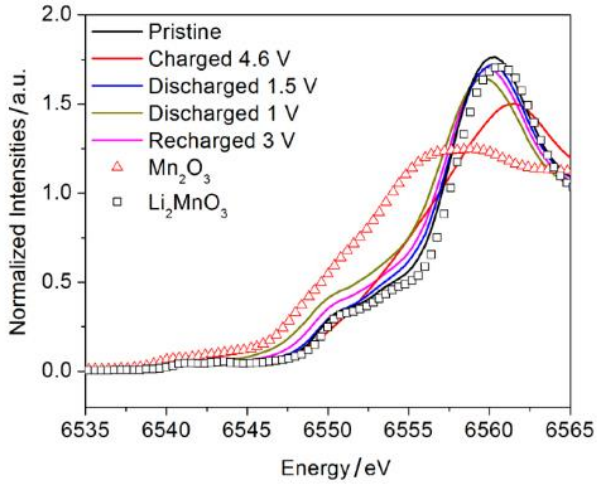

Figure S4. The selected normalized Mn K-edge XANES spectra of $Li_2Ru_{0.5}Mn_{0.5}O_3$ collected during the first cycle and the second charge process, with Mn_2O_3 (Aigma-Aldrich, 99%) and Li_2MnO_3 (800 ^oC synthesis[7]) as references.

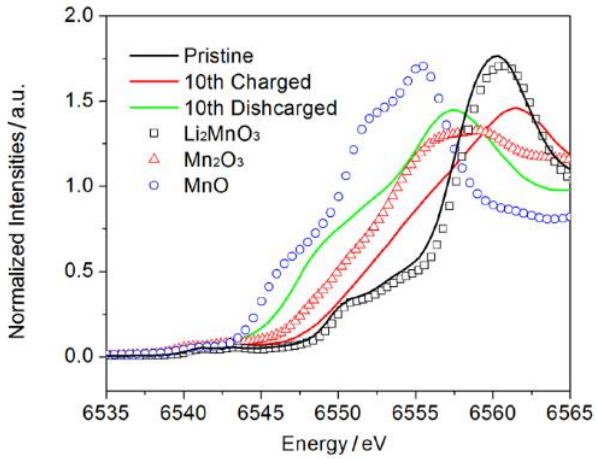

Figure S5. The selected normalized *ex situ* Mn K-edge XANES spectra of $Li_2Ru_{0.5}Mn_{0.5}O_3$ collected at 10th charged and discharged states, with MnO (Sigma-Aldrich, 99%), Mn_2O_3 (Sigma-Aldrich, 99%) and Li_2MnO_3 (800 ^oC synthesis[4]) as references.

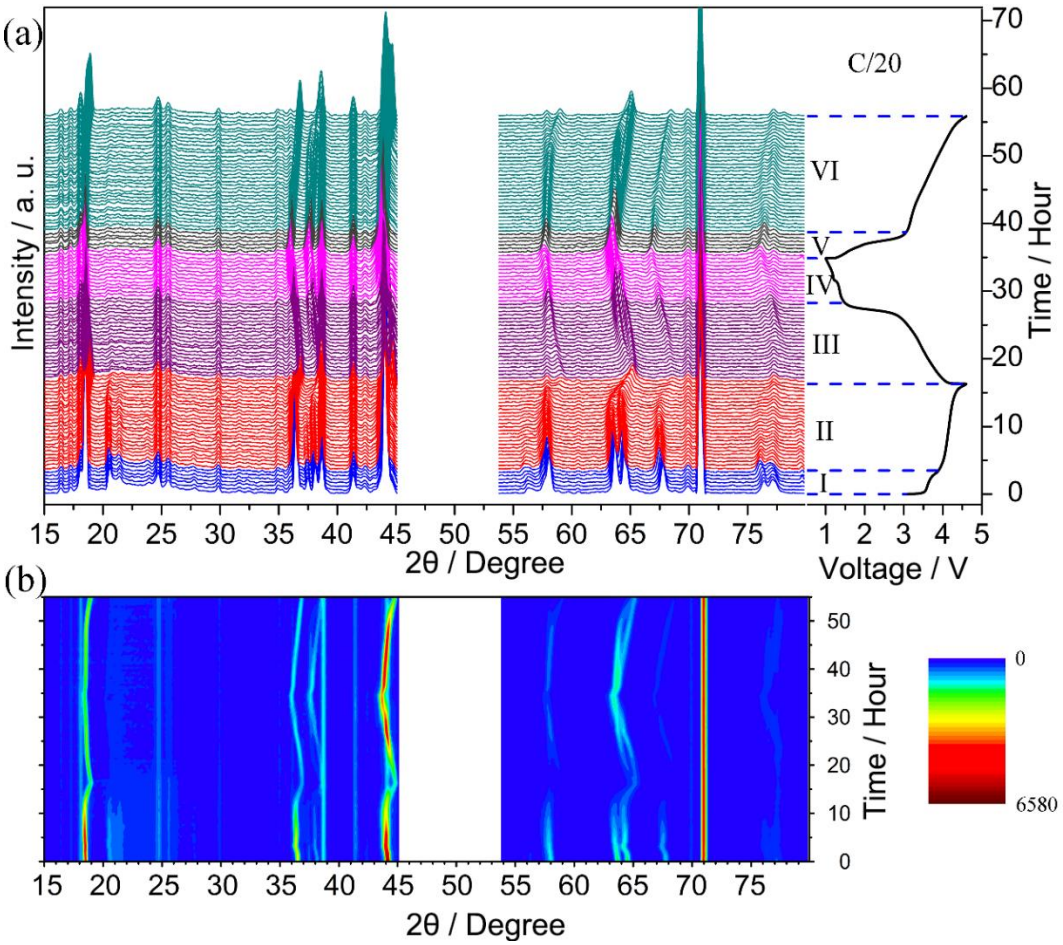

Figure S6. (a) The *in situ* XRD patterns of $Li_2Ru_{0.5}Mn_{0.5}O_2$ between 4.6 and 1 V *vs.* Li^+/Li at a

current rate of C/20. The right side is the charge discharge curve of $Li_2Ru_{0.5}Mn_{0.5}O_3$/Li cell. (b) 2D contour plot of peak intensities as a function of reaction time.

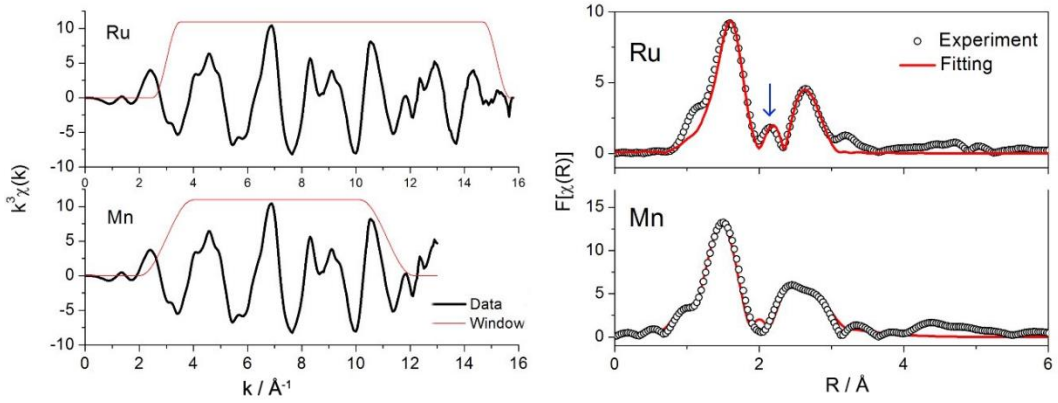

Figure S7. (left) k^3-weighted $\chi(k)$ EXAFS signals for $Li_2Ru_{0.5}Mn_{0.5}O_3$ in the pristine state; (right) Least-square fits of experimental EXAFS spectra. The fitting parameters are summarized in Table S1.

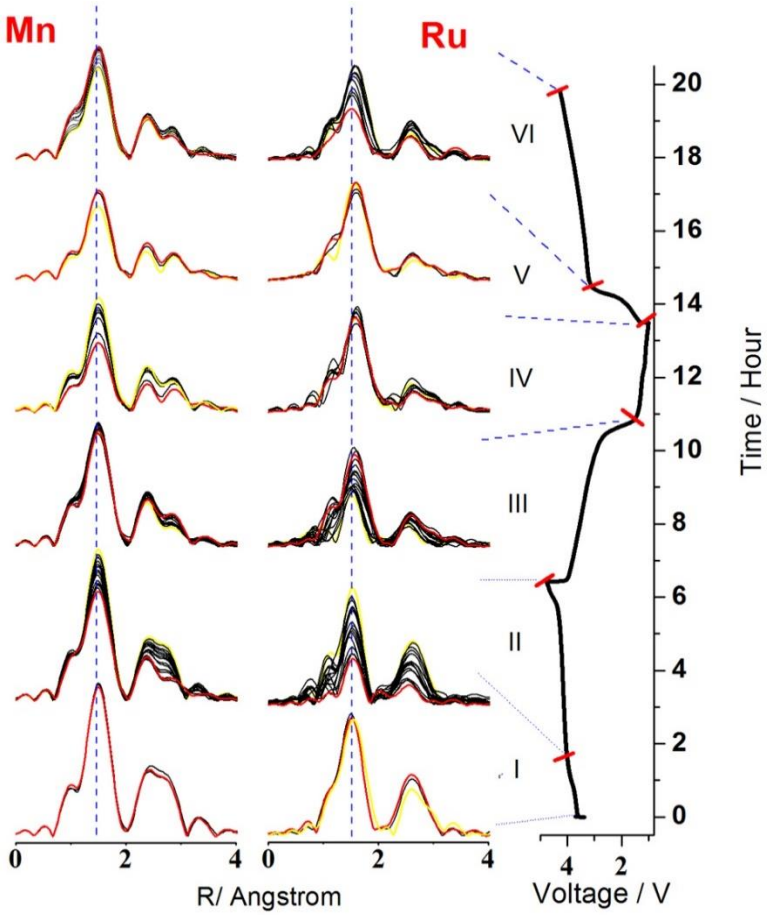

Figure S8. The k^3-weighted $\chi(k)$ EXAFS signals at Mn K-edge and Ru K-edge for $Li_2Ru_{0.5}Mn_{0.5}O_3$ collected during the first cycle and the second charge process between 4.6 and 1.0 V *vs.* Li^+/Li at a rate of 1/8 C. k range from 3 to 11.15 Å and 3.2 to 13 Å was chosen for Fourier transfer of the $\chi(k)$ EXAFS signals for Mn and Ru respectively.

Table S1. Parameters obtained from Least-squares fits of experimental EXAFS spectra acquired at Mn and Ru K-edge of as-prepared $Li_2Ru_{0.5}Mn_{0.5}O_3$

	Mn	**Ru**
k range	3 - 11.32 $Å^{-1}$	3 - 15.198 $Å^{-1}$
R range	1 - 3.2 Å	1.156 - 3 Å
R factor	0.008	0.003
S_0^2	0.8	0.75
E_0	-1.82 ± 1.97 eV	4.86 ± 1.81eV
R_{eff}		
M-O	1.916 ± 0.014 Å	2.012 ± 0.009 Å
M-M_1		2.587 ± 0.022 Å
M-M_2	2.849 ± 0.022 Å	2.939 ± 0.024 Å
M-M_3	3.135 ± 0.034 Å	3.050 ± 0.039 Å
σ^2		
M-O	0.0033 ± 0.0009 $Å^2$	0.0034 ± 0.0006 $Å^2$
M-M_1	/	0.0029 ± 0.0018 $Å^2$
M-M_2	0.0018 ± 00029 $Å^2$	0.0021 ± 0.0028 $Å^2$
M-M_3	0.0032 ± 0.0044 $Å^2$	0.0059 ± 0.0050 $Å^2$

■ REFERENCE

1. Sathiya, M.; Ramesha, K.; Rousse, G.; Foix, D.; Gonbeau, D.; Prakash, A. S.; Doublet, M. L.; Hemalatha, K.; Tarascon, J. M., High Performance $Li_2Ru_{1-y}Mn_yO_3$ ($0.2 \leq y \leq 0.8$) Cathode Materials for Rechargeable Lithium-Ion Batteries: Their Understanding. *Chem. Mater.* **2013,** *25* (7), 1121-1131.
2. Newville, M., IFEFFIT: interactive XAFS analysis and FEFF fitting. *J. Synchrotron Rad.* **2001,** *8* (2), 322-324.
3. Hammersley, A. P.; Svensson, S. O.; Hanfland, M.; Fitch, A. N.; Hausermann, D., Two-dimensional detector software: From real detector to idealised image or two-theta scan. *High Pressure Research* **1996,** *14* (4-6), 235-248.
4. Juhas, P.; Davis, T.; Farrow, C. L.; Billinge, S. J. L., PDFgetX3: a rapid and highly automatable program for processing powder diffraction data into total scattering pair distribution functions. *J. Appl. Crystallogr.* **2013,** *46* (2), 560-566.
5. Momma, K.; Izumi, F., VESTA: a three-dimensional visualization system for electronic and structural analysis. *J. Appl. Crystallogr.* **2008,** *41* (3), 653-658.

6. Yu, X.; Lyu, Y.; Gu, L.; Wu, H.; Bak, S.-M.; Zhou, Y.; Amine, K.; Ehrlich, S. N.; Li, H.; Nam, K.-W.; Yang, X.-Q., Understanding the Rate Capability of High-Energy-Density Li-Rich Layered Li1.2Ni0.15Co0.1Mn0.55O2 Cathode Materials. *Adv. Energy Mater.* **2014,** *4* (5), 1300950.
7. Wang, R.; He, X.; He, L.; Wang, F.; Xiao, R.; Gu, L.; Li, H.; Chen, L., Atomic Structure of Li_2MnO_3 after Partial Delithiation and Re-Lithiation. *Adv. Energy Mater.* **2013,** *3* (10), 1358-1367.